Available online at www.sciencedirect.com
SCIENCE DIRECT®
Journal of Nuclear Materials 348 (2006) 26–32
journal of nuclear materials
www.elsevier.com/locate/jnucmat

Proton transfer in $SrCeO_3$-based oxide with internal reformation under supply of CH_4 and H_2O

Satoshi Fukada *, Shigenori Suemori, Ken Onoda

Department of Applied Quantum Physics and Nuclear Engineering, Kyushu University, Hakozaki 6-10-1, Higashi-ku, Fukuoka 812-8581, Japan

Received 5 April 2005; accepted 3 August 2005

Abstract

Mass and charge transfer in a proton-conducting ceramic with internal reformation under the supply of $CH_4 + H_2O$ was experimentally investigated for application to a fuel detritiation system of a fusion reactor. The oxide used in the present experiment was $SrCe_{0.95}Yb_{0.05}O_{3-a}$, and the electrodes were composed of Ni–SiO_2 paste and Ni wire mesh. The system was described by $CH_4 + H_2O|Ni|SrCe_{0.95}Yb_{0.05}O_{3-a}|NiO|O_2 + H_2O$. Plots of the I–V (electric current density versus cell potential) characteristic curve were determined under the conditions of different H_2O/CH_4 concentration ratios and temperatures of 600–800 °C. It was found that the system could work well even without any external CH_4 reformer. Mass-transfer process in/on the porous Ni electrode and in the ceramic electrolyte was experimentally clarified. The distribution of carbon depositions in the porous electrode was also determined with EDX by scanning over entire surface in the scope of SEM. The ratio of CH_4 to H_2 direct decomposition to its steam-reforming reaction was found to be different from location to location in the porous Ni electrode.

1. Introduction

Some doped perovskite-type oxides exhibit proton conduction at higher temperatures. $SrCeO_3$- or $CaZrO_3$-based oxides demonstrated higher proton-conducting performance at 600–1000 °C [1]. Therefore, uses for a hydrogen pump, a hydrogen sensor and a hydrogen (or tritium) purifier operated at higher temperatures are expected in the nuclear engineering field, especially in the tritium recovery process of a fusion reactor. Previously, hydrogen extraction from H_2–H_2O gas mixtures was experimentally investigated for a blanket tritium recovery system or a fuel detritiation system in a fusion reactor [2,3]. It was clarified there that $SrCeO_3$- and $CaZrO_3$-based ceramics can work as a hydrogen pump when an over-potential corresponding to polarization at electrodes was applied to them. However, their researches focused mainly on the action of hydrogen pumping. It was not made clear where the rate-determining step is and whether or not the ceramics can work for the decomposition of CH_4, which is another target molecule in the tritium recovery process of a fusion reactor.

* Corresponding author. Tel.: +81 92 642 4140; fax: +81 92 642 3800.
E-mail address: sfukada@nucl.kyushu-u.ac.jp (S. Fukada).

0022-3115/$ - see front matter © 2005 Elsevier B.V. All rights reserved.
doi:10.1016/j.jnucmat.2005.08.002

From a viewpoint of proton conductivity, a Sr–Ce–Yb oxide was more advantageous than Sr–Zr–Yb and Ca–Zr–In oxides. However, some Ce-based ceramics decomposed to $SrCO_3$ and CeO_3 under a dense CO_2 atmosphere [4], which is a large disadvantage for the application of the proton-conducting ceramic to industrial use. In the present study, a gas mixture of CH_4 and H_2O was introduced into the anode cell of $SrCe_{0.95}Yb_{0.05}O_{3-a}$ with a porous Ni electrode, which also works as an internal reformer of CH_4 to H_2. A gas mixture of O_2 and H_2O was supplied to a cathode cell. The present system was considered a realistic way in order to avoid disposing to a high CO_2 atmosphere. There were other reasons to select and experiment the system composed of the $SrCe_{0.95}Yb_{0.05}O_{3-a}$ and the porous Ni electrodes: The first, it was considered a good way to convert CH_4 to H_2 in the neighborhood of electrodes because of simplicity. Reforming CH_4 to H_2 on the Ni electrode and producing direct electric power from CH_4 as a fuel cell can be achieved by both actions of steam reformation on the Ni electrode and proton conduction in the ceramic. It was expected that the porous Ni electrode can work as an internal reformer. The second reason, the Ni electrode was non-reactive to CO, which is a by-product of the steam-reforming reaction. Therefore high reactivity to CH_4 was expected.

In the present study, a fuel-cell system was set up to study an overall mass-transfer process including the CH_4 reformation and proton conduction, because the fuel-cell system is preferable to the fuel detritiation process from a viewpoint of the basic study of mass transfer in the cell. Mass and charge transfer process in the $SrCe_{0.95}Yb_{0.05}O_{3-a}$ cell with Ni electrodes was investigated from a standpoint of chemical engineering field. A gas mixture of CH_4 and H_2O was introduced into the ceramic cell system without any additional CH_4 reformer. There was no experimental study on whether or not the present system can work as a fuel cell or a fuel detritiation system, characteristic I–V curves were determined in the system of $CH_4 + H_2O|Ni|SrCe_{0.95}Yb_{0.05}O_{3-a}|NiO|O_2 + H_2O$. These results were compared with previous results obtained under the condition where a gas mixture of $H_2 + H_2O$ was supplied to a similar cell system composed of $SrCe_{0.95}Yb_{0.05}O_{3-a}$ and porous Ni electrodes [5]. Surfaces on the anode electrode after experiment were observed for the analysis of carbon deposition using a scanning electron microscope (SEM) and an energy dispersive X-ray spectroscopy (EDX).

2. Experimental

Fig. 1 shows a schematic diagram of the experimental apparatus tested as a fuel-cell system. Anode and cathode cells were enclosed in upper and lower 316 stainless-steel flanges with 50 mm in diameter. Anode and cathode gas supply lines were attached to respective cells. A ceramic plate of $SrCe_{0.95}Yb_{0.05}O_{3-a}$ was placed between the two flanges. In order to avoid gas leaking out the cells, a glass gasket was used as a shield material between the ceramic and the flanges. The ceramic plate was 15 mm in diameter and 3.5 mm in thickness. A Ni paste composed of Ni powder and SiO_2 solution (Aremco Products, Pyro-Duct 598) and a Ni wire mesh were attached to both surfaces of the ceramic. The pasted Ni electrode was calcined at 1000 °C. Its thickness was estimated 100 μm based on a SEM photo. Before experiment, the anode electrode was reduced by a H_2 gas flow for sufficient time at 800 °C. This was because the Ni electrode after calcination was oxidated. The anode gas supply line was connected to CH_4 and Ar gas cylinders through mass flow meters and water bubblers to the anode cell. In a similar way, the O_2 gas line was connected to the cathode cell. Water vapor was added to CH_4 and O_2 streams by bubblers. The bubblers were immersed in a constant-temperature bath that was

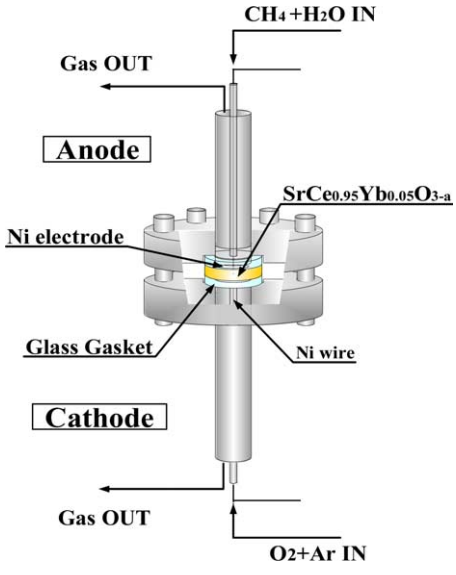

Fig. 1. A schematic diagram of the experimental apparatus for ceramic fuel-cell system.

controlled to a specified temperature. All gas lines after bubblers were heated up to around 100 °C to avoid water condensing.

A gas mixture of CH_4, H_2O and Ar was introduced into the anode cell under a constant flow rate. The inlet CH_4 concentration was 10.0%, the H_2O concentration was 5.0%, 10%, or 20%, and balance gas was Ar. The total gas flow rate was 50 cm^3 (NTP)/min throughout the experiment. A gas mixture of O_2 and H_2O was introduced into the cathode cell. The inlet H_2O concentration was 20%, and the rest was O_2. The total gas flow rate was also 50 cm^3 (NTP)/min. The electric current and cell potential were measured by the two-terminal method using a data acquisition system (Keithley Co. Ltd., type 2700). The outlet gas component from the anode cell was measured by gas chromatography that could detect H_2, O_2, CO, CO_2, CH_4 and other hydrocarbons. A water condenser was installed in a midway location from the anode cell to the gas chromatography to avoid water influent.

The internal and surfaces of the porous Ni electrode were investigated by SEM, and the distribution of carbon deposits in the electrode was determined by EDX. The element on material surfaces was determined by scanning over the entire surface in the scope of SEM.

3. Results

3.1. I–V curve

Fig. 2 shows examples of the *I–V* (electric current density versus cell potential) characteristic curves for the $CH_4 + H_2O|Ni|SrCe_{0.95}Yb_{0.05}O_{3-a}|NiO|\ O_2 + H_2O$ system at 800 °C. There was small difference in the *I–V* curves for different H_2O concentrations. The *V* value at a specified *I* value was the largest at the highest H_2O concentration. The cell potential diminished slightly with the decrease of the H_2O concentration. The whole *I–V* curve was correlated to the linear relation of $V = E_0 - IR$. The slope of the *I–V* curve corresponds to the overall resistance denoted by *R*, which found to be almost independent of the H_2O concentration. On the other hand, difference in the intercept of the vertical axis denoted by E_0 diminished a little with the decrease of the H_2O concentration. The open circuit voltage was 0.914 V at 20% H_2O, 0.871 V at 10% and 0.852 V at 5%. This difference was attributable to the difference in the H_2 partial pressure on the anode Ni electrode. The apparent H_2 pressure in the anode cell,

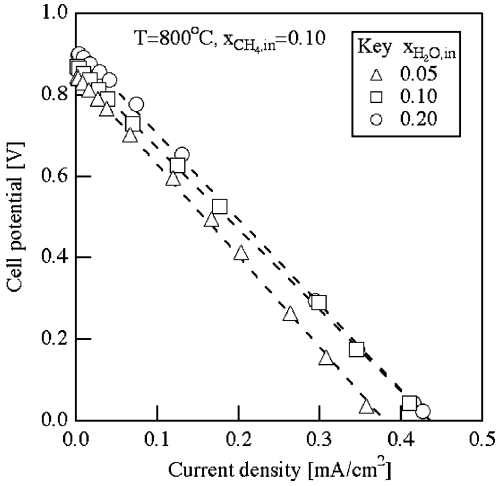

Fig. 2. *I–V* curves for different H_2O concentrations in the system of $CH_4 + H_2O|Ni|SrCe_{0.95}Yb_{0.05}O_{3-a}|NiO|O_2 + H_2O$.

$p_{H_2,anode}$, was calculated using the following Nernst equation [6]:

$$E_0 = -\frac{\Delta G_{H_2O}}{2F} + \frac{R_g T}{2F} \ln\left(\frac{p_{H_2,anode}\, p_{O_2,cathode}^{0.5}}{p_{H_2O,cathode}}\right) \qquad (1)$$

The estimated $p_{H_2,anode}$ values were 6.4×10^3, 2.5×10^3 and 1.7×10^3 Pa for the three anode H_2O concentrations at 800 °C and were almost in proportion to the anode H_2O concentration.

Fig. 3 shows the dependence of the *I–V* curve on temperature under the condition of a constant H_2O concentration in the anode. Apparently, the slope

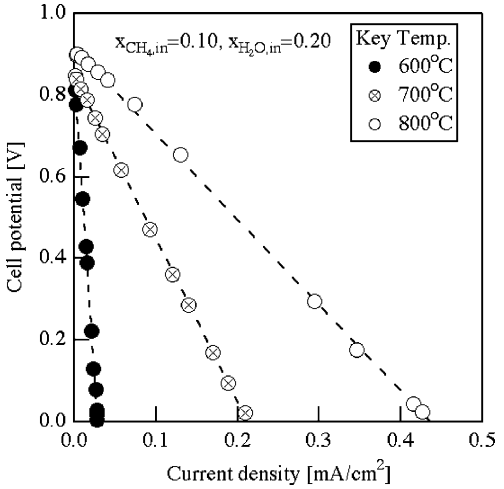

Fig. 3. *I–V* curves for different temperatures in the system of $CH_4 + H_2O|Ni|SrCe_{0.95}Yb_{0.05}O_{3-a}|NiO|O_2 + H_2O$.

decreased with the elevation of temperature. Linearity was also held regardless of the different temperature conditions. The intercept was slightly changed depending on the different temperatures. Judging from these experimental results, it was considered that the difference in E_0 was attributable to the different H_2 partial pressures on the anode electrode. It was calculated that the apparent H_2 pressure was 2.3×10^2 Pa at 600 °C, 5.7×10^2 Pa at 700 °C and 6.4×10^3 Pa at 800 °C. The dependence of $p_{H_2,anode}$ on temperature was close to that of the overall conductivity, as discussed in the following section.

Fig. 4 shows an Arrhenius plot of the overall conductivity values for the $CH_4 + H_2O|Ni|SrCe_{0.95}Yb_{0.05}O_{3-a}|NiO|O_2 + H_2O$ system. The overall conductivity denoted by σ was determined by the relation of $\sigma = \frac{L}{RS}$. Here, L is the thickness of the ceramic electrolyte, and S is the surface area.

The σ values depended on only temperature and were independent of the anode H_2O vapor pressure. The σ values of the $H_2 + H_2O|Ni|SrCe_{0.95}Yb_{0.05}O_{3-a}|NiO|O_2 + H_2O$ system are also shown in the figure for comparison. The activation energy under the condition of the $CH_4 + H_2O$ supply was 106 kJ/mol and was larger than that for the $H_2 + H_2O$ supply (75.6 kJ/mol). The absolute σ values for the $CH_4 + H_2O$ supply were over ten times smaller than those for the $H_2 + H_2O$ supply.

The concentrations of CO and H_2 as well as CH_4 at the outlet of the anode cell were detected by the gas chromatography analysis. The CO_2 concentration was less than the CO_2 detectable level of 10 ppm. There was no hydrocarbon except for CH_4 throughout the experiment. Therefore it was not considered that CO_2 affected the present fuel-cell system.

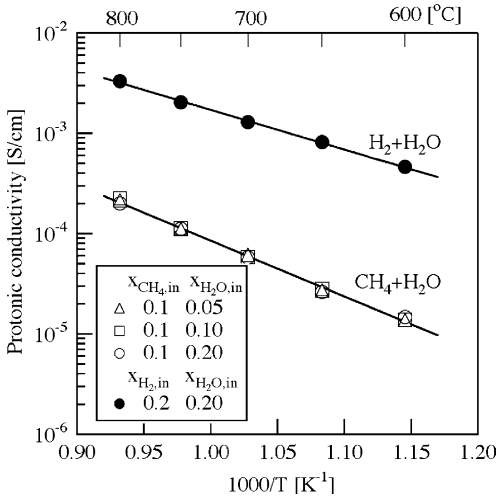

Fig. 4. Temperature dependence of overall conductivity in systems of $CH_4 + H_2O|Ni|SrCe_{0.95}Yb_{0.05}O_{3-a}|NiO|O_2 + H_2O$ and $H_2 + H_2O|Ni|SrCe_{0.95}Yb_{0.05}O_{3-a}|NiO|O_2 + H_2O$.

3.2. Carbon distribution in electrode

SEM and EDX were used to investigate carbon deposited in/on the porous anode electrode. Three different locations on the surface were investigated; (A) on the porous Ni surface, (B) on the Ni mesh in the electrode, and (C) at the interface between the Ni electrode and the ceramic electrolyte. Several SEM photos at the locations of (A)–(C) are shown in Fig. 5(A)–(C). Two specific EDX spectra for the entire scope of SEM at the positions (B) and (C) are shown in Fig. 5(D) and (E). Elements of Si, Ni and O in the former and those of Sr, O, C and Ni in the latter were observed. The atomic ratio of O/Sr determined from the EDX spectrum (E) was near to three of the stoichiometric value. The amount of carbon deposits determined is compared in Table 1. As seen in the table, almost all carbon deposits were distributed at the interface between the electrode and the electrolyte. No carbon deposit was present on the Ni electrode surface. We concluded from the results as follows. The steam-reforming reaction was the major process on the electrode surface. Some CH_4 diffused through the porous Ni electrode, and some CH_4 decomposition occurred at the narrow interface between the electrode and electrolyte. This may be because of depletion of the H_2O concentration in the porous electrode with compensation for steam-reforming reaction. Dark spheres seen in Fig. 5(C) seemed to be carbon deposits. Therefore, we tried to obtain EDX spectrum at an extended specific spot to investigate where carbon was localized on the ceramic surface. However, we could not identify it specifically in a more extended SEM scope, because of the low electric conductivity of the ceramic. The carbon deposition did not affect the mass and charge transport in the ceramic and electrodes. This was because the fuel-cell performance did not change regardless of experimental times.

4. Discussion

4.1. Rate-determining step

Based on the above experimental results, we will discuss which of either reaction processes on the

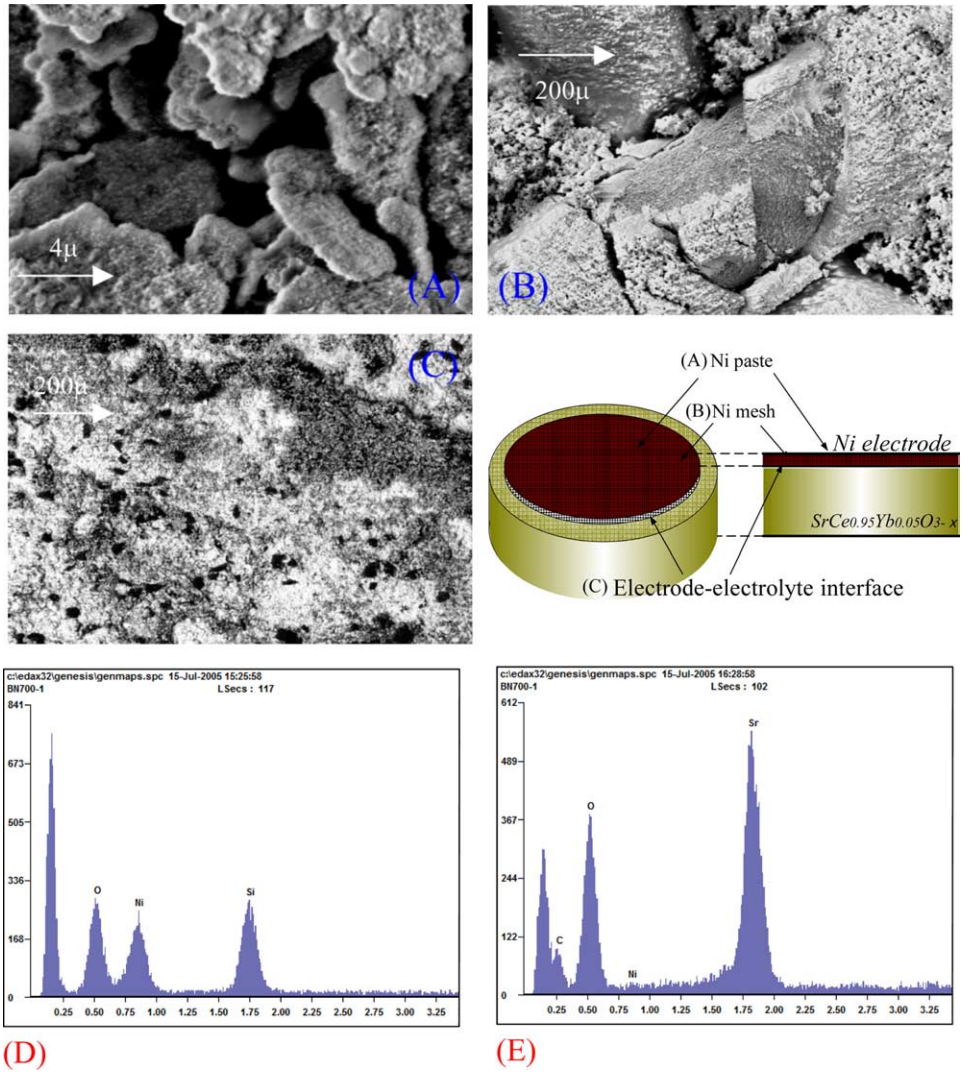

Fig. 5. SEM photo and EDX spectrum at interface between ceramics electrolyte and Ni electrode (A) ×5000, (B) ×100, (C) ×100, (D) EDX spectrum at position (B), (E) EDX spectrum at position (C).

Table 1
Carbon deposition at different locations in electrode and electrolyte

Component	Electrode surface	Internal of electrode	Interface of electrode–electrolyte
Carbon	0.0 (wt%)	1.87	24.3
Oxygen	12.0	15.2	17.6
Nickel	88.0	82.9	3.0

anode and cathode electrodes or proton conduction through the ceramic is the rate-determining step.

When the gas mixture of CH_4 and H_2O was introduced into the anode cell, two competing reactions may occur on the Ni surface:

$$CH_4 \rightleftarrows C + 2H_2 \quad (2)$$

$$CH_4 + H_2O \rightleftarrows CO + 3H_2 \quad (3)$$

The two reactions are composed of several elementary steps such as $CH_4 + 2* \rightarrow CH_3^* + H^*$, $CH_3^* + * = CH_2^* + H^*$ and so on [7]. The asterisk (*) signifies an empty adsorption site and chemical formulae with an asterisk do adsorbed species. The reaction rate of Eq. (2) was of the first-order on the CH_4 concentration [8]. That of Eq. (3) was of the first-order on the CH_4 concentration and of the first-order on the H_2O concentration [9]. The ideal conversion ratio of the two reactions from CH_4 to H_2 was calculated using the Gibbs free-energy changes of Eqs. (2) and (3) in a thermodynamic table [10]. Fig. 6 shows

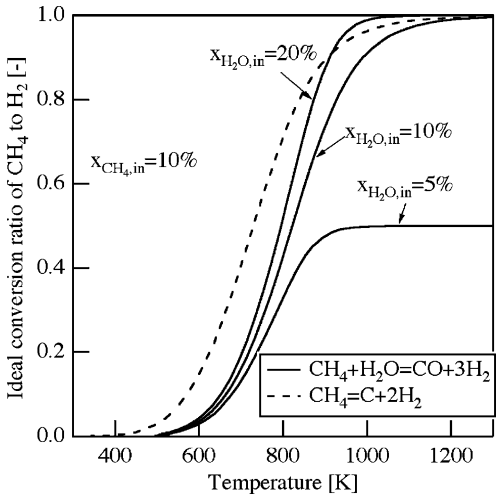

Fig. 6. Ideal conversion ratio of CH_4 to H_2 calculated from Gibbs free-energy change.

the calculation results. The solid and broken lines mean the maximum reaction yield. This is because the outlet gas was assumed to be under an equilibrium condition. Judging from the two reaction-rate constants previously determined [8,11], the reaction of Eq. (2) was comparatively slower. Therefore, the broken line in the figure may be overestimated. On the other hand, the reaction rate of Eq. (3) was comparatively faster. Therefore, it was probable that the reaction yield of the solid line may be realistic ones. Another reaction of $CH_4 + 2H_2O \rightleftarrows CO_2 + 4H_2$ or $CO + H_2O \rightleftarrows CO_2 + H_2$ can occur also on the Ni surfaces judging from the Gibbs free-energy change [10]. However, since $CO_2$was not detected at the outlet of the anode cell, it was considered that the above reaction could be neglected.

After H_2 produced on the anode electrode diffused through the ceramic electrolyte, the following reactions occurred at the cathode interface between the NiO electrode and the ceramic:

$$2H^+ + (1/2)O_2 \rightleftarrows H_2O + 2h^+ \quad (4)$$

$$2H^+ + O_O^X \rightleftarrows H_2O + V_{\ddot{O}} \quad (5)$$

Since a sufficient amount of H_2O was supplied to the cathode cell, it was probable that the formation of the oxygen vacancy ($V_{\ddot{O}}$) on the cathode interface was suppressed. Consequently, proton conduction became a major process in this experiment. The effects of the hole (h^+) and the oxide ion (O_O^X) conductions could be neglected. Therefore, the activation energy of σ in the case of the $H_2 + H_2O$ supply condition should correspond to that of the proton conduction through the ceramic. It was also consistent with our previous experiment carried out by means of cole–cole plots [5] as well as the proton conductivity determined previously [4]. It is concluded that the rate-determining step of the mass- and charge-transfer under the condition of the $H_2 + H_2O$ supply is the charge-transfer process on the cathode electrode.

The cell potential on the vertical axis in Figs. 2 and 3 corresponded to the overall difference in potential between the anode and cathode cells. Therefore, it included all of the polarities at the anode and cathode. The cathode cells, under the conditions of the $CH_4 + H_2O$ and $H_2 + H_2O$ supply, were under the same condition. Consequently, the difference in the activation energy between the conditions of the $CH_4 + H_2O$ and $H_2 + H_2O$ supply should correspond to the polarity of the anode side. The difference in the activation energy was 30 kJ/mol. The value was in close agreement with the activation energy of the reaction-rate constant of steam-reforming reaction [9]. The experimental fact that the $p_{H_2,anode}$ values estimated from E_0 using Eq. (1) were in proportion to the anode H_2O concentration supported the idea of the steam-reforming reaction being predominant on the anode, because the steam-reforming reaction is of the first-order on the H_2O concentration. Based on these experimental results, it is concluded that the proton-conducting $SrCe_{0.95}Yb_{0.05}O_{3-a}$ ceramic with Ni electrodes could also work under the conditions of the $CH_4 + H_2O$ supply as well as the $H_2 + H_2O$ supply. The absolute value of the apparent protonic conductivity under the condition of the $CH_4 + H_2O$ supply was around ten times lower than that of the H_2–H_2O supply. This is because the reaction rate of CH_4 water-reforming on the Ni electrode was lower than that of the dissociation of H_2 to $2H^+ + 2e^-$.

4.2. Application to tritium recovery system

$SrCe_{0.95}Yb_{0.05}O_{3-a}$ ceramic will work less efficiently as a fuel cell for the power generation of vehicles because of lower protonic conductivity than polymer electrolyte membranes. YSZ is also a promising material for stationary fuel cells working at higher temperature, and its oxide ion conductivity is around 0.1 S/cm. Judging from these results, $SrCe_{0.95}Yb_{0.05}O_{3-a}$ ceramics do not seem to exhibit attractive performance as a fuel cell for power

generation. On the other hand, there are several advantages to use for a tritium recovery system. First, only hydrogen or tritium can be extracted from gas mixtures at 600–800 °C and diffuses through the ceramics. In the anode side tritium is oxidized to tritium water vapor that is easily recovered by a molecular sieve adsorbent. Next, the proton conductivity of the ceramics showed high linearity regardless of electric current. Therefore, simple mechanism and high stability for CH_4 reformation and H_2 extraction exhibited expected properties for application to a blanket tritium recovery system or a fuel detritiation system of a fusion reactor system.

As another possible application, a hydrogen or methane sensor is promising as an in-line monitor under moist atmosphere at higher temperature. The E_0 value will be a good indication of the H_2 or CH_4 partial pressure.

5. Conclusions

The cell system of $CH_4 + H_2O|Ni|SrCe_{0.95}Yb_{0.05}O_{3-a}|NiO|O_2 + H_2O$ could work well under the condition of the $CH_4 + H_2O$ gas mixture supply without any additional CH_4 reformer. Only the CH_4 steam-reforming reaction occurred on the surface under the proper H_2O/CH_4 concentration ratio and no carbon deposited on the surfaces of the Ni electrode. However, some CH_4 diffused through the porous Ni electrode and the direct decomposition reaction occurred at the interface between the ceramic electrolyte and the electrode. Only hydrogen diffused through the ceramic and reacted with O_2 in the cathode cell. The rate-determining step was the CH_4 reformation reaction on anode electrode. The proton conductivity was independent of the anode H_2O vapor pressure. The apparent H_2 partial pressure estimated from the cell potential at open circuit was in proportion to the H_2O vapor pressure in the anode cell because the reaction rate is of the first-order on the H_2O pressure. Since the carbon deposition inside the anode electrode did not affect the I–V characteristic curve during the present experiment, the $SrCe_{0.95}Yb_{0.05}O_{3-a}$ ceramic will work as a tritium recovery system of a fusion reactor system.

References

[1] H. Iwahara, Solid State Ionics 77 (1995) 289.
[2] Y. Kawamura, S. Konishi, M. Nishi, Fus. Sci. Technol. 45 (2004) 33.
[3] M. Tanaka, K. Katahira, Y. Asakura, T. Uda, H. Iwahara, I. Yamamoto, J. Nucl. Sci. Technol. 41 (2004) 61.
[4] T. Scherban, A.S. Nowick, Solid State Ionics 35 (1989) 189.
[5] S. Fukada, K. Onoda, S. Suemori, J. Nucl. Sci. Technol. 41 (2005) 1.
[6] A.J. Bard, L.R. Faulkner, Electrochemical Methods: Fundamentals and Applications, 2nd Ed., New York, Wiley, 2000.
[7] I. Alstrup, J. Catal. 151 (1995) 216.
[8] S. Fukada, N. Nakamura, J. Monden, M. Nishikawa, J. Nucl. Mater. 329–333 (2004) 1365.
[9] W. Jin, X. Gu, S. Li, P. Huang, N. Xu, J. Shi, Chem. Eng. Sci. 55 (2000) 2617.
[10] O. Kubaschewski, C.E. Alcock, Metallurgical Thermochemistry, 5th Ed., Pergamon, New York, 1979.
[11] S. Fukada, N. Nakamura, J. Monden, Int. J. Hydrogen Energy 29 (2004) 619.